Stall Recovery Guidance Algorithms Based on Constrained Control Approaches

Vahram Stepanyan [1]
University of California Santa Cruz, Santa Cruz, CA 95064

Kalmanje Krishnakumar [2], John Kaneshige [3], and Diana Acosta [4]
NASA Ames Research Center, Moffett Field, CA 94035

Aircraft loss-of-control, in particular approach to stall or fully developed stall, is a major factor contributing to aircraft safety risks, which emphasizes the need to develop algorithms that are capable of assisting the pilots to identify the problem and providing guidance to recover the aircraft. In this paper we present several stall recovery guidance algorithms, which are implemented in the background without interfering with flight control system and altering the pilot's actions. They are using input and state constrained control methods to generate guidance signals, which are provided to the pilot in the form of visual cues. It is the pilot's decision to follow these signals. The algorithms are validated in the pilot-in-the loop medium fidelity simulation experiment.

I. Introduction

Aircraft loss-of-control (LOC), in particular approach to stall or fully developed stall, is a major factor contributing to the aircraft safety risks. Recent high profile accidents, such as the crash of

[1] Senior Research Scientist, University Affiliated Research Center, NASA Ames Research Center/Mail Stop 269/1, AIAA Senior Member, email: vahram.stepanyan@nasa.gov
[2] Autonomous Systems and Robotics Branch Chief, Intelligent Systems Division, NASA Ames Research Center/Mail Stop 269/1, AIAA Associate Fellow, email: kalmanje.krishnakumar@nasa.gov
[3] Researcher, Intelligent Systems Division, NASA Ames Research Center/Mail Stop 269/1, Member AIAA, email: john.t.kaneshige@nasa.gov
[4] Researcher, Intelligent Systems Division, NASA Ames Research Center/Mail Stop 269/1, Member AIAA, email: diana.m.acosta@nasa.gov

Continental Connection flight 3407 and Air France flight 447 (see [27, 30] for details), have resulted in growing concerns in the international aviation community about the pilots failure to recognize conditions that lead to aerodynamic stall and ability to respond appropriately to an unexpected stall or upset event [8]. To address these concerns, as well as the recommendations of the study of 18 recent loss-of-control events by the Commercial Aviation Safety Team (CAST), the Federal Aviation Administration (FAA) issued final rule changes to 14 CFR Part 121 (see [3] for details) mandating air carriers in the United States to train the pilots in recognizing, avoiding, and properly recovering from stalls by 2019.

This pilot training assumes availability of proper aerodynamic models representing realistic approach to stall, stall and post-stall flight conditions, and high fidelity simulators capable of reproducing these flight conditions. To this end, a linearized unsteady vortex lattice method was combined with a decambering viscous correction to study the impact of unsteady and post-stall aerodynamics on a maneuvering aircraft [28]. In [26], wind-tunnel data and sensor characteristics were used to identify aerodynamic models for simulating stall and recovery for transport aircraft. In [1], development of a type-representative model is presented to meet the randomness requirement typically available in stall and post-stall flight conditions. The evaluation of several full stall simulator models in piloted simulations is presented in [32].

In addition, FAA has issued the Advisory Circular AC 120-109 (see [2] for details), which eliminates recovery profiles that emphasizes minimal altitude loss and the immediate translation to the maximum thrust, and emphasizes immediate reduction of angle of attack as the main step in the stall recovery procedure. However, FAA does not provide guidance for full aerodynamic stall recovery. In addition, the CAST "Safety Enhancement SE 207" research initiative propose the aerospace community to develop algorithms to enhance pilots situational awareness and provide control guidance for recovery from aerodynamic stall [36].

In recent years, the development of LOC detection and mitigation algorithms for transport aircraft in hazardous conditions, such as atmospheric disturbances, airframe impairment or component failures, was substantially influenced by the NASA Aeronautics Research Mission Directorate (ARMD) Vehicle Safety Systems Technologies (VSST) project. An overview of on-board LOC

prevention and recovery technologies can be found in [5]. Since parametric uncertainties and unknown atmospheric disturbances are accompanying the LOC events, adaptive control methods were proposed for aircraft LOC prevention and recovery, see for example [15], [23], [40], [7] and references therein. Other approaches include neural network estimations combined with sliding mode control [35] or trajectory optimization techniques [39], actuator health monitoring combined with robust control methods [18, 29], state-limiting augmentation to a dynamic inversion control [12], constrained nonlinear model predictive control [19], pseudo-control hedging [21], multi-mode upset recovery flight control [11], flight envelope protection system [38], just to mention few of them. However, theses methods shift the ultimate decision making authority from the pilot to the automation, alter the exiting flight control system, and may not be implemented on-board in the near future.

Another focus area of VSST was to assist the crew for accurate decision-making under hazardous conditions by increasing the situational awareness. On-line estimation of the safe flight envelope is one of the directions in this area, see for example [14, 22, 24, 25, 41] and references therein. To estimate the flight envelope of impaired aircraft an algorithm based on the differential vortex lattice method combined with an extended Kalman filter is presented in [25]. In [22], the safe maneuvering envelope is estimated using time scale separation and optimal control formulation for the reachability analysis. This approach is extended in [41] to include uncertainty quantifications. In [24], the computation of recoverable sets for aircraft in LOC condition is presented using approximations of safe sets for the closed-loop linearized system dynamics.

These safe flight envelopes are used to improve the pilot's situational awareness by determining available aircraft maneuverability or controllability margins using the optimal control framework [14], adaptive estimation [34] or data-based predictive control [4]. The controllability boundaries are computed using the pilot's inputs, aircraft state time histories recorded over a time window, and the estimated dynamics, and are provided to the pilot in the form of two dimensional bounding box around the pilot's stick current position.

The pilots situational awareness can also be improved by conducting nonlinear analysis of the aircraft dynamics for identification of the bifurcation points on the boundary of safe envelop, see for example [13, 20, 33] and references therein. In [20], it is shown that dynamic nonlinearities

result in difficult or nonintuitive regulation around the critical trim points or transitioning between them because of non-uniqueness of corresponding control actions. The bifurcation analysis are used to identify the attractors of the nonlinear aircraft that govern the upset behavior in [13], and to determine feasible level flight trim points as a function of elevator deflection for several thrust and leading edge flap settings [33].

Although presented LOC detection, estimation and mitigation methods have some preventive functionality, they do not address the stall recovery guidance problems, which is a critical component in flight safety assurance, given that the aerodynamic stall can happen in any pitch attitude or bank angle or at any airspeed even for a nominal aircraft.

In this paper we present several algorithms to address the stall recovery guidance problem. These algorithms are implemented in the background without interfering with the flight control system and altering the pilot's actions. They are using input and state constrained control methods to generate guidance signals, which are provided to the pilot in the form of visual cues. It is the pilot's decision to follow this signals. The algorithms are validated in the pilot-in-the loop medium fidelity simulation experiment.

II. Stall Recovery Guidance Problem Formulation.

When the aircraft approaches stall or is in stall, the pilots main step in the recovery procedure should be directed to reducing the angle of attack, as the FAA Advisory Circular recommends. This is done mainly by commanding pitch down maneuver using the longitudinal control effectors. To predict the aircraft response to such commands, the pilot needs to have easily understandable and meaningful information about the state variables, which are directly influenced by or influencing the dynamic behavior of the angle of attack, since the latter is not directly controlled by the pilot. From this perspective, we use the flight path angle, the altitude and the pitch angle.

On the other hand, the information provided to the pilot must be predictive in nature in order to give some lead time to the pilot to make a right decision in stressful situation. That is the current values of the corresponding state variables may not be useful from the recovery perspective, since they may represent unsafe flight conditions. Therefore, it is necessary to develop predictive models

to generate the aircraft state predictions, which coincide with the actual states for nominal (safe) flight conditions. When the aircraft leaves the safe flight envelop, these models continue to generate signals corresponding to safe flight conditions, hence can guide the pilot to recover the aircraft.

In this paper, our objective is to develop algorithms for generating stall recovery guidance signals, which have physical meanings and are easy to understand, can increase the pilots situational awareness, can be easily visualized on the primary flight display with simple symbology and color codes, and are not overburdening or impacting the pilot from fulfilling the mission.

III. Preliminaries

A. Pseudo Control Hedging

The principle of Pseudo Control Hedging (PCH) was originally developed in [17] in the context of Model Reference Adaptive Control (MRAC) to compensate for discrepancy resulting from the actuator position or rate saturation. The purpose of the PCH was to modify the reference model dynamics such that the actuator characteristics are removed from the tracking error dynamics. Therefore the adaptation mechanism, which is based on the tracking error, is not affected by the saturation. The PCH method was successfully applied to non-adaptive flight controls in conjunction with the nonlinear dynamic inversion (NDI) (see for example [21] and references therein), thus providing an alternative for the inversion of the actuator dynamics. Here, we outline the PCH framework from the aircraft control perspective. Let the aircraft dynamics be given by

$$\dot{x}(t) = f(x) + g(x)u_{com}(t)\,, \tag{1}$$

where $u_{com}(t)$ is the commanded control input to the actuator, $f(x)$ is the aerodynamic model and $g(x)$ is the control effectiveness. The NDI control law is given by

$$u_{com}(t) = g^{-1}(x)[v(t) - a(x)]\,, \tag{2}$$

where $v(t)$ is the virtual input representing the desired dynamics. The actual control input $u_{act}(t)$ entering the aircraft dynamics may not be identical with the commanded input $u_{com}(t)$ due to actuator characteristics. Therefore the estimate of the virtual input $\hat{v}(t)$ is computed as

$$\hat{v}(t) = f(x) + b(x)u_{act}(t)\,. \tag{3}$$

The PCH signal is obtained from (2) and (3) as

$$\tilde{v}(t) = v(t) - \hat{v}(t)\,. \tag{4}$$

This signal is used to modify the reference model dynamics, which is given by

$$\dot{x}_{ref}(t) = -a_m x_{ref}(t) + b_m x_{com}(t) - \tilde{v}(t)\,, \tag{5}$$

where $x_{com}(t)$ is the external (pilot's) command. Denoting the tracking error by $e(t) = x(t) - x_{ref}(t)$, we obtain

$$\begin{aligned} \dot{e}(t) &= f(x) + g(x)u_{act}(t) + a_m x_{ref}(t) - b_m x_{com}(t) - \tilde{v}(t) \\ &= f(x) + g(x)u_{com}(t) + a_m x_{ref}(t) - b_m x_{com}(t)\,, \end{aligned} \tag{6}$$

which is exactly the error dynamics without the actuator in the loop. When aerodynamic model and control effectiveness are uncertain, an adaptive NDI is used, where the uncertainties are estimated on-line and are taken into account in the computation of the PCH signal.

B. Flight Envelope Protection Method

This approach was introduced in [37] and applied to NASA Transport Class Model as a flight envelop protection method, which modifies the pilots input when the corresponding output variable approaches the envelop boundary. Let the state of the aircraft to be protected satisfy the equation

$$x^{(m)}(t) = f(x) + g(x)u_{com}(t)\,, \tag{7}$$

where $u_{com}(t)$ is the pilot's command, $f(x)$ and $g(x)$ represent the aircraft aerodynamic model, and m is the relative degree from the command to output of the system. Let the safe flight envelope is given by the inequality

$$x(t) \leq x_{\max} \tag{8}$$

for all $t \geq 0$. As soon as the inequality (8) is violated, the command $u_{com}(t)$ is modified such that $x(t)$ tracks the output $x_{ref}(t)$ of a reference model

$$x_{ref}^{(m)}(t) = -a_{m-1}x_{ref}^{(m-1)}(t) - \cdots - a_0\left[x_{ref}(t) - x_{\max}\right]\,, \tag{9}$$

which is initialized at the system's initial conditions. The envelope violation is detected by means of the comparison signal

$$w(t) = -a_{m-1}x^{(m-1)}(t) - \cdots - a_0 \left[x(t) - x_{\max}\right] , \tag{10}$$

and the pilot's command is modified as follows

$$u_{com}(t) = \begin{cases} u_{com}(t), & \text{if } u_{com}(t) < \frac{1}{g(x)} \left[w(t) - f(x)\right] \\ \frac{1}{g(x)} \left[x_{ref}^{(m)}(t) - f(x)\right], & \text{if } u_{com}(t) \geq \frac{1}{g(x)} \left[w(t) - f(x)\right] \end{cases} . \tag{11}$$

At the command modification time instant, the initial conditions of the reference model are reset to the system's states. It is shown in [37] that the command modification (11) with the initial condition resetting guarantees the inequality (8), if the impulse response $h(t)$ of the reference model satisfies the condition

$$0 \leq \int_0^t h(\tau)d\tau \leq 1 \tag{12}$$

for all $t \geq 0$, which implies that the reference model is constructed to be non-overshooting (for the non-overshooting control the reader is referred to [6], [9], [10], [31], and references therein).

IV. Approaches to Stall Recovery Guidance

In this section we present several approaches to the stall recovery guidance problem. Our focus is on the aircraft longitudinal dynamics. The development of stall recovery guidance algorithms for aircraft full dynamics is subject of the future research.

A. Input Constrained Control Approach

This approach is based on the PCH method, where the angle of attack is treated as a control signal, and the role of the actuator is played by a magnitude saturation block. The lower and upper limits of this block are the α-envelop boundaries, which are available from the manufacturer for the nominal aircraft or are obtained by means of the envelop estimation methods presented in Section I. The idea is to generate a guidance signal, which matches with the corresponding actual variable for nominal flight conditions and provides a recovery cue to the pilot, when the angle of attack reaches the stall value (some margins may be applied to give a lead time to the pilot). Next, we discuss the

application of this idea to generate recovery guidance signals for several aircraft states, which can be easily visualized on the primary flight display (PFD) without overloading.

1. Flight path angle guidance

Consider the following flight path angle dynamics

$$\dot{\gamma}(t) = \frac{1}{mV}\left[L\cos\mu + S\sin\mu - mg\cos\gamma + T\left(\sin\alpha\cos\mu + \sin\beta\cos\alpha\sin\mu\right)\right], \tag{13}$$

where γ is the flight path angle, m is the mass, g is the gravity acceleration, V is the airspeed, L is the lift force, S is the side force, μ is the wind axis bank angle, T is the thrust, α is the angle of attack, and β is the sideslip angle. The dynamics (13) are used as a model for generation of the guidance signal, which is implemented in the on-board computer in real time, where all variables except for L and γ are computed from the actual measurements and aerodynamic model lookup table. The lift force is represented in the form

$$L = L_0 + L_\alpha \alpha\,, \tag{14}$$

where the coefficients L_0 and L_α are computed from the aerodynamic model lookup table for each time instant. Therefore the dynamics for the γ-guidance model can be represented as

$$\dot{\gamma}_{guid}(t) = f_\gamma(x) + g_\gamma(x)\alpha_{com}(t)\,, \tag{15}$$

where

$$\begin{aligned} f_\gamma(x) &= \frac{1}{mV}\left[L_0\cos\mu + S\sin\mu - mg\cos\gamma_{guid} + T\left(\sin\alpha\cos\mu + \sin\beta\cos\alpha\sin\mu\right)\right] \\ g_\gamma(x) &= \frac{1}{mV}L_\alpha\cos\mu\,. \end{aligned} \tag{16}$$

In this setup, α in the term $T\left(\sin\alpha\cos\mu + \sin\beta\cos\alpha\sin\mu\right)$ is the actual angle of attack and is treated as an external variable to the guidance model (15). This enables us to stay within the affine in the control framework, and is justified by the fact that the contribution of the thrust in the flight path angle dynamics is very small compare to the lift force.

Here, our goal is to design a control input $\alpha_{com}(t)$ such that the guidance model (15) tracks the reference model

$$\dot{\gamma}_{ref}(t) = k_\gamma\left[\gamma_{act}(t) - \gamma_{ref}(t)\right], \tag{17}$$

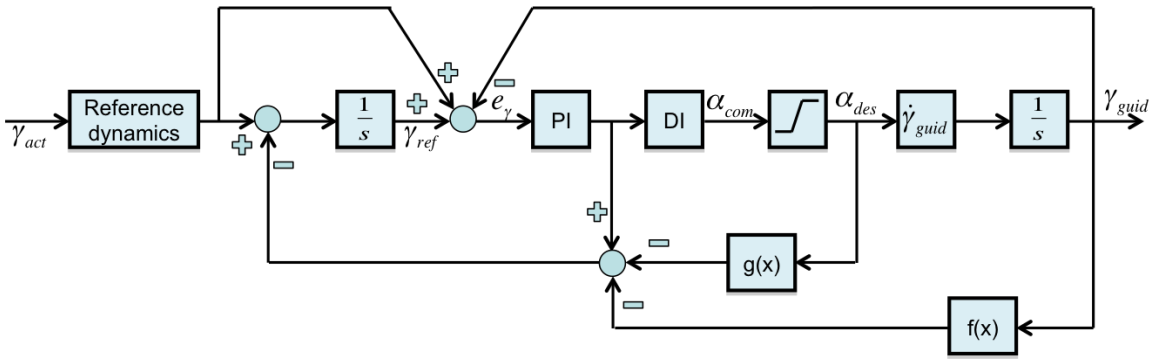

Fig. 1 The schematics of the flight path angle guidance design.

where $\gamma_{act}(t)$ is the aircraft actual flight path angle, and k_γ is a design parameter representing the time constant of the reference model. We design a NDI control as

$$\alpha_{com}(t) = g_\gamma^{-1}(x)\left[v(t) - f_\gamma(x)\right] , \tag{18}$$

and PCH signal as

$$\tilde{v}(t) = v(t) - f_\gamma(x) - g_\gamma(x)\alpha_{des}(t) , \tag{19}$$

where $\alpha_{des}(t)$ is the output of the saturation block, and $v(t)$ is the virtual control, which is computed as

$$v(t) = -k_p e_\gamma(t) - k_i \int_0^t e_\gamma(t)dt + k_\gamma\left[\gamma_{act}(t) - \gamma_{ref}(t)\right] . \tag{20}$$

Here, k_p and k_i are the proportional and integral gains, $e_\gamma = \gamma_{guid}(t) - \gamma_{ref}(t)$ is the tracking error, and the reference model dynamics are modified according to PCH method

$$\dot{\gamma}_{ref}(t) = k_\gamma\left[\gamma_{act}(t) - \gamma_{ref}(t)\right] - \tilde{v}(t) . \tag{21}$$

The schematics of the design is presented in Figure 1. The resulting tracking error dynamics have the form

$$\dot{e}_\gamma(t) = -k_p e_\gamma(t) - k_i \int_0^t e_\gamma(t)dt . \tag{22}$$

It is straightforward to show that $\gamma_{guid}(t)$ always tracks the reference flight path angle $\gamma_{ref}(t)$. The later in turn tracks the actual flight path angle as long as $\alpha_{com}(t)$ remains in the safety limits. When the aircraft approaches to stall or is in stall, $\alpha_{com}(t)$ exits the safety limits. Then the algorithm

modifies $\gamma_{ref}(t)$ such that the corresponding $\alpha_{com}(t)$ returns to the safety limits. In this case, $\gamma_{ref}(t)$ no longer tracks the command to the reference model, which is the actual flight path angle. The resulting $\gamma_{guid}(t)$ indicates a safe flight condition, and is displayed on PFD. It can be seen as a small magenta ball inside the flight path symbol in nominal conditions (see Figure 2).

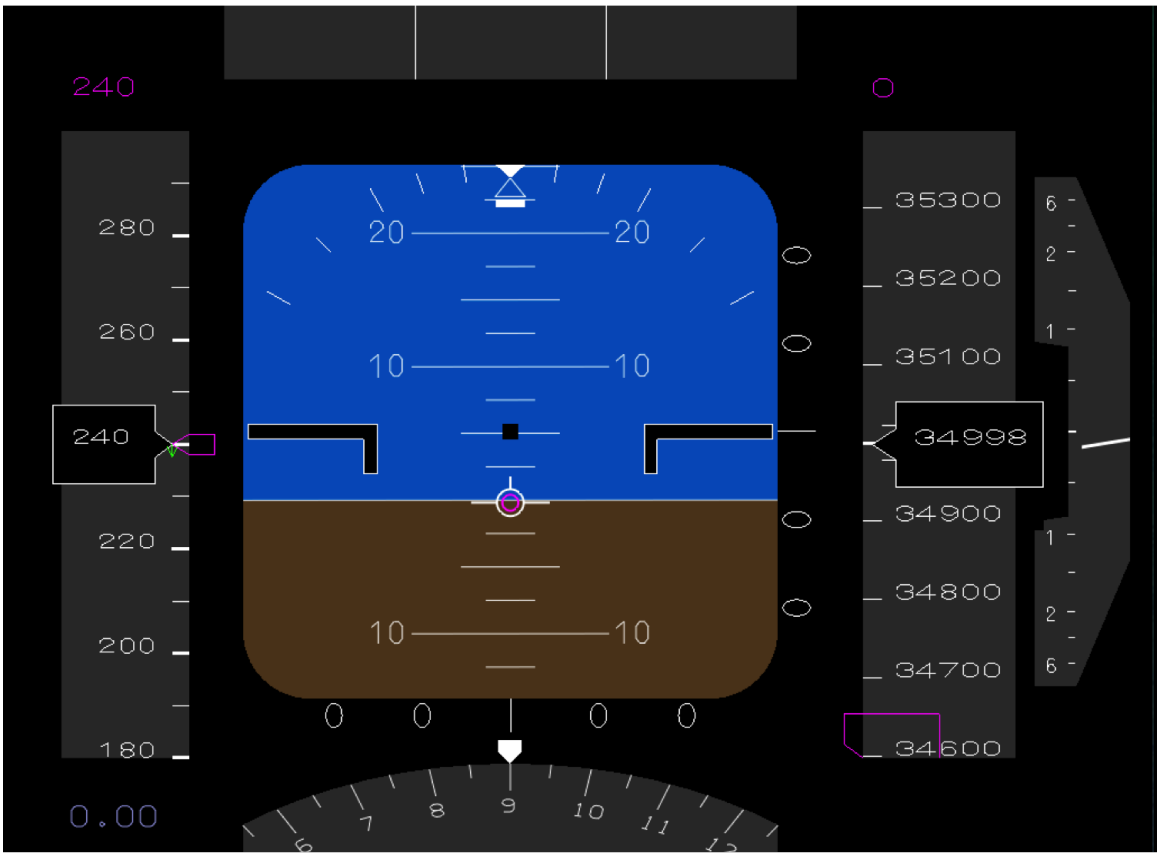

Fig. 2 PFD with the flight path angle guidance signal in a nominal condition.

As soon as $\alpha_{com}(t)$ hits the saturation limits, the magenta ball separates from the flight path symbol (see Figure 3), but still indicates a safe flight condition.

2. Altitude guidance

Consider the following altitude dynamics

$$\ddot{h}(t) = \frac{1}{m}\left[-Z - mg + T\sin\theta\right], \tag{23}$$

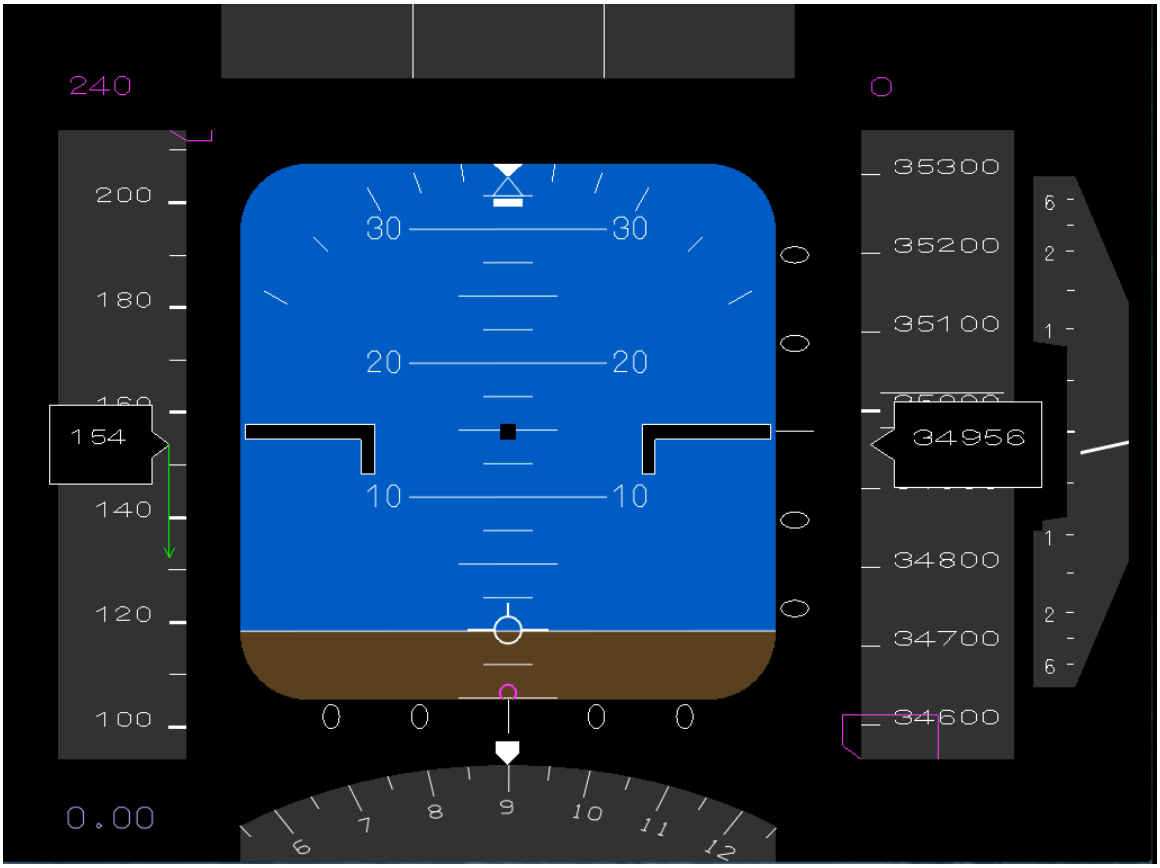

Fig. 3 PFD with the flight path angle guidance signal in approach to stall condition.

where h is the altitude, Z is the aerodynamic force component on the inertial z direction (North-East-Down frame), and θ is the pitch angle. For the h-guidance model we use the representation

$$Z = Z_0 + Z_\alpha \alpha \,, \tag{24}$$

where the coefficients Z_0 and Z_α are computed from the aerodynamic model lookup table for each time instant. The dynamics for the h-guidance model have the form

$$\ddot{h}_{guid}(t) = f_h(x) + g_h(x)\alpha_{com}(t) \,, \tag{25}$$

where we denote

$$\begin{aligned} f_h(x) &= \frac{1}{m}\left[Z_0 - mg + T\sin\theta\right] \\ g_h(x) &= \frac{1}{m} Z_\alpha \,. \end{aligned} \tag{26}$$

Again, we treat the term $T\sin\theta$ independent of the control input $\alpha_{com}(t)$, and use the measurement of actual pitch angle to compute it.

Here, we design a control input $\alpha_{com}(t)$ such that the guidance model (25) tracks the second order reference model

$$\ddot{h}_{ref}(t) = -k_1 \dot{h}_{ref}(t) - k_2 \left[h_{ref}(t) - h_{act}(t)\right] , \tag{27}$$

where $h_{act}(t)$ is the aircraft actual altitude, and $k_1,\ k_2$ are design parameters representing the characteristics of the reference model. In this case, the design is based on the following equations

$$\begin{aligned} \alpha_{com}(t) &= g_h^{-1}(x)\left[v(t) - f_h(x)\right] \\ v(t) &= -k_1 \dot{e}_h(t) - k_2 e_h(t) + \ddot{h}_{ref}(t) \\ \tilde{v}(t) &= v(t) - f_h(x) - g_h(x)\alpha_{des}(t) , \end{aligned} \tag{28}$$

where $e_h(t) = h_{guid}(t) - h_{ref}(t)$ is the tracking error. The resulting modified reference model dynamics are

$$\ddot{h}_{ref}(t) = -k_1 \dot{h}_{ref}(t) - k_2 \left[h_{ref}(t) - h_{act}(t)\right] - \tilde{v}(t) . \tag{29}$$

As in the flight path angle case, $h_{guid}(t)$ tracks the actual altitude as long as $\alpha_{com}(t)$ remains in the safety limits. When the aircraft approaches to stall or is in stall, $\alpha_{com}(t)$ leaves the safety limits, triggering nonzero $\tilde{v}_h(t)$, which modifies the reference signal $h_{ref}(t)$ such that $\alpha_{com}(t)$ returns to the safety limits. However, the resulting $h_{guid}(t)$ no longer tracks the actual altitude, but indicates a safe flight condition. Figure 4 displays the altitude guidance signal as a magenta bar on the altitude tape in nominal flight conditions. It can be observed that the guidance signal coincides with the aircraft actual altitude.

Figure 4 displays the altitude guidance signal in stall condition, where the magenta bar indicates a lower altitude for the recovery from stall.

B. State Constrained Control Approach

One of the primary variables controlled by the pilot and readily available on the PFD is the aircraft pitch angle. Hence, it can be a good guidance signal candidate for the stall recovery algorithm. However, the pitch angle is not a good stall indicator, although it relates to the angle of attack through aircraft state variables. In fact, stall can happen in any pitch attitude. One way

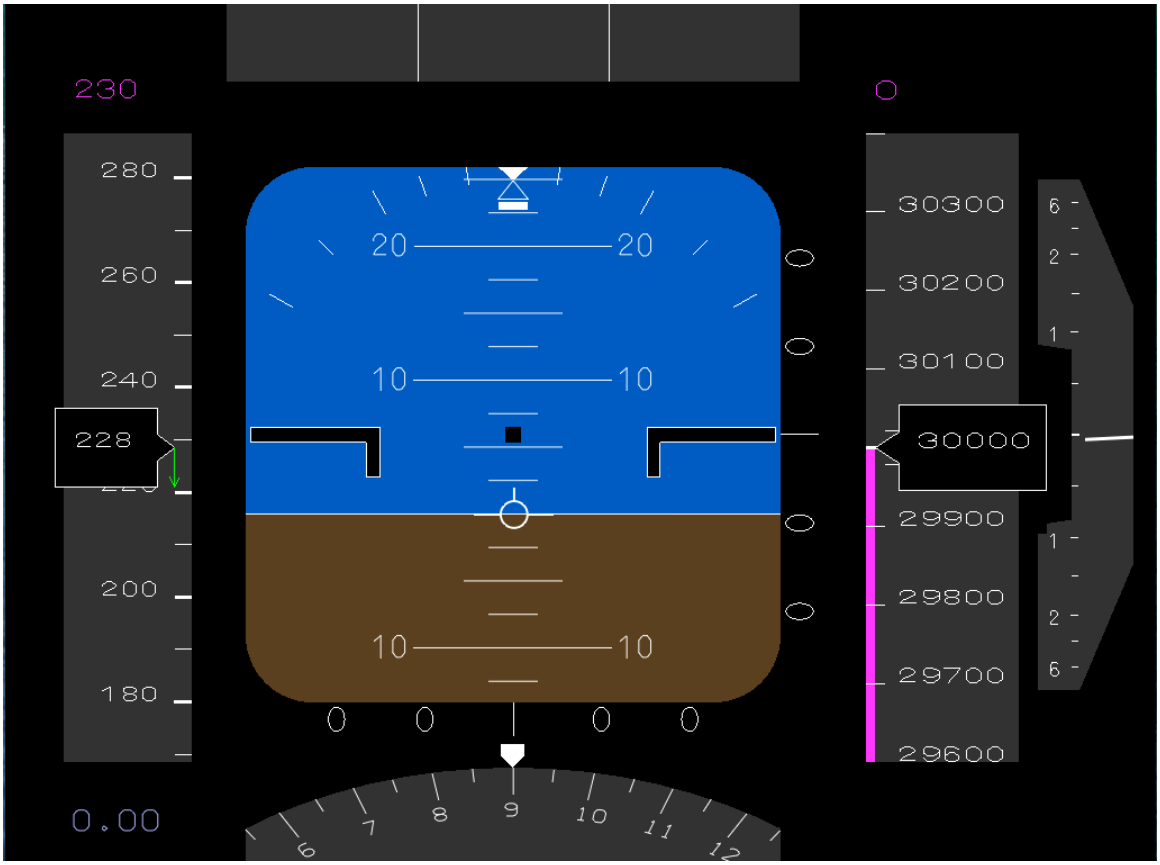

Fig. 4 PFD with the altitude guidance signal in approach to stall condition.

to use the pitch angle for the guidance purposes is to derive a proper pitch rate signal trough the following angle of attack dynamics

$$\dot{\alpha}(t) = q - f(x, \alpha)\,, \tag{30}$$

where

$$f(x, \alpha) = \sec\beta \left[\frac{1}{mV}\left(L - mg\cos\gamma\cos\mu + T\sin\alpha\right) + p\cos\alpha\sin\beta + r\sin\alpha\sin\beta\right]$$

and $p,\ q,\ r$ are body frame angular rates, and integrate the kinematic equation

$$\dot{\theta}(t) = q\cos\phi - r\sin\phi\,, \tag{31}$$

where ϕ is the body frame bank angle. To this end, the dynamics (30) is used to generate a guidance model with a properly designed external command, for which q is treated as a control input. The output of the guidance model is kept within the α-envelope using state limiting control methods. The resulting control signal indicates a safe pitch rate for all flight conditions, and matches with

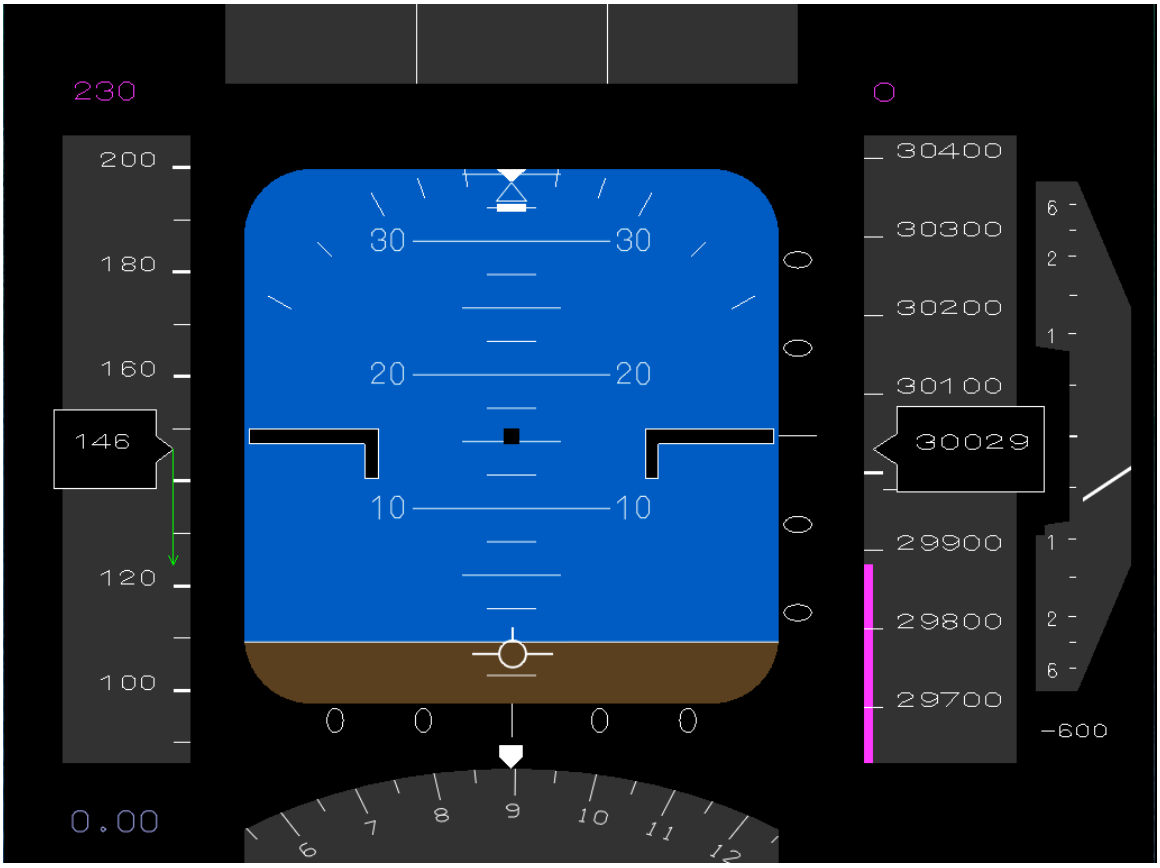

Fig. 5 PFD with the altitude guidance signal in approach to stall condition.

the actual pitch rate for the nominal one. Therefore, the corresponding pitch angle obtained from (31) can provide a stall recovery guidance to the pilot.

The guidance model in this case is mimicking the angle of attack dynamics

$$\dot{\alpha}_{guid}(t) = q_{com}(t) - f(x, \alpha_{guid})\,, \tag{32}$$

where $q_{com}(t)$ is treated as a control input, and is designed such that $\alpha_{guid}(t)$ tracks the actual angle of attack for normal flight regimes. That is we set

$$q_{com}(t) = -k_\alpha[\alpha_{guid}(t) - \alpha(t)] + f(x, \alpha_{guid}) + q - f(x, \alpha)\,, \tag{33}$$

which results in exponentially stable dynamics

$$\dot{e}_\alpha(t) = -k_\alpha e_\alpha(t) \tag{34}$$

for the error signal $e_\alpha(t) = \alpha_{guid}(t) - \alpha(t)$. Here $k_\alpha > 0$ is a design parameter representing the convergence rate. Initializing the guidance model at the actual angle of attack guarantees

$\alpha_{guid}(t) = \alpha(t)$ for al $t \geq 0$ as long as the control input $q_{com}(t)$ satisfies (33). When the aircraft approaches to stall, $q_{com}(t)$ needs to be modified to represent a guidance signal for the recovery. If we directly follow the envelope protection method from [37], that is if we choose a reference model

$$\dot{\alpha}_{ref}(t) = -k_\alpha[\alpha_{ref}(t) - \alpha_{max}]\,, \tag{35}$$

where α_{max} is the stall angle (possibly with some buffer to give the pilot a lead time), and use the upper comparison signal

$$w_u(t) = -k_\alpha[\alpha_{guid}(t) - \alpha_{max}] \tag{36}$$

to modify $q_{com}(t)$ according to equation

$$q_{com}(t) = \begin{cases} q_{com}(t), & \text{if } q_{com}(t) < w_u(t) + f(x, \alpha_{guid}) \\ \dot{\alpha}_{ref}(t) + f(x, \alpha_{guid}), & \text{if } q_{com}(t) \geq w_u(t) + f(x, \alpha_{guid}) \end{cases}, \tag{37}$$

and reset the initial conditions to $\alpha_{ref}(t_u) = \alpha_{guid}(t_u)$ at the command switch time instant t_u, we end up with $\alpha_{guid}(t) \leq \alpha_{max}$. Therefore, the corresponding $q_{com}(t)$ will represent a safe flight condition, but not a suitable recovery signal. In essence, the signal $\alpha_{guid}(t)$ as well as the actual angle of attack is anticipated to leave the envelope boundary represented by α_{max}, when its rate of change exceeds the limit set by the comparison signal. The command modification (37) forces the signal $\alpha_{guid}(t)$ to follow the reference $\alpha_{ref}(t)$ instead of the actual angle of attack.

This motivates us to change the reference model driving signal such that the resulting $\alpha_{ref}(t)$ converges to a target value α_t instead of α_{max} after its rate of change increase is detected at time t_u. That is we set

$$\dot{\alpha}_{ref}(t) = -k_\alpha[\alpha_{ref}(t) - \alpha_t] \tag{38}$$

for $t \geq t_u$. Here, the target angle of attack value $\alpha_t < \alpha_{max}$ is chosen from the linearity region on the lift curve to recover the controllability of the aircraft. For example it can be set to the trim value corresponding to the current flight conditions. Since $\alpha_{ref}(t_u) \leq \alpha_{max}$, and the reference model is non-overshooting and non-undershooting, we can conclude that $\alpha_t \leq \alpha_{ref}(t) \leq \alpha_{max}$ for all $t \geq t_u$. When the rate of change of $\alpha_{guid}(t)$ drops below the lower comparison signal

$$w_l(t) = -k_\alpha[\alpha_{guid}(t) - \alpha_t] \tag{39}$$

at some time instant t_l, the control input is reset to (33) with $\alpha_{guid}(t_l) = \alpha(t_l)$. In the interval $[t_u\ t_l]$ the reference signal $\alpha_{ref}(t)$ monotonically changes from $\alpha_{guid}(t_u)$ to α_t, and the guidance model tracks it. The resulting $q_{com}(t)$ generates a guidance signal for the aircraft pitch angle according to equation

$$\dot{\theta}_{guid}(t) = q_{com}(t)\cos\phi - r\sin\phi\,. \tag{40}$$

In this case, the flight director stile symbols can be used to display the recovery guidance signal. Figure 6 displays the pitch angle guidance signal as a magenta lines on both sides of PFD in nominal condition, which are aligned with the actual pitch angle display.

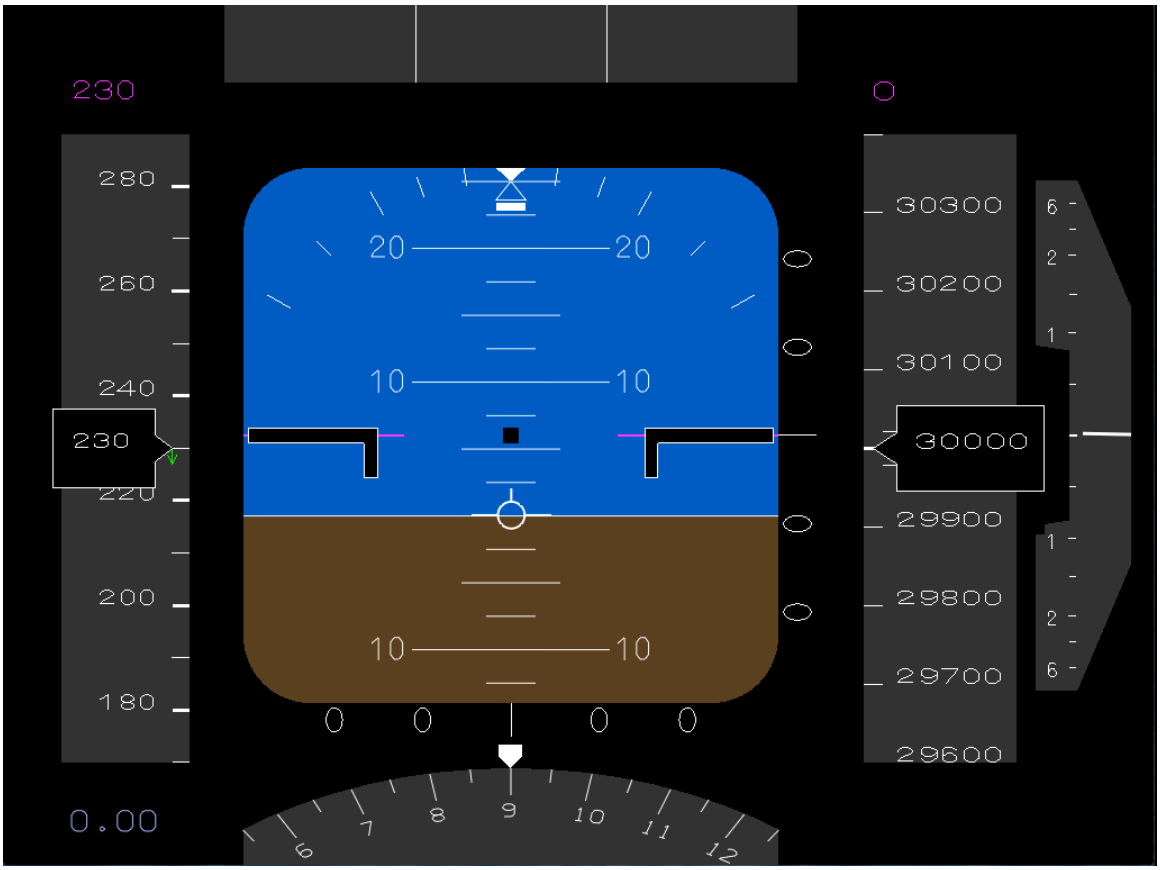

Fig. 6 PFD with the pitch angle guidance signal (magenta line) in nominal condition.

Figure 7 displays the pitch angle guidance signal on PFD in stall condition. The magenta lines indicate that the pilot should pitch down in order to recover from the stall.

We summarize the state constrained control based stall recovery guidance algorithm as follows

- Run the guidance model (32) with the initial condition $\alpha_{guid}(0) = \alpha(0)$ and control input

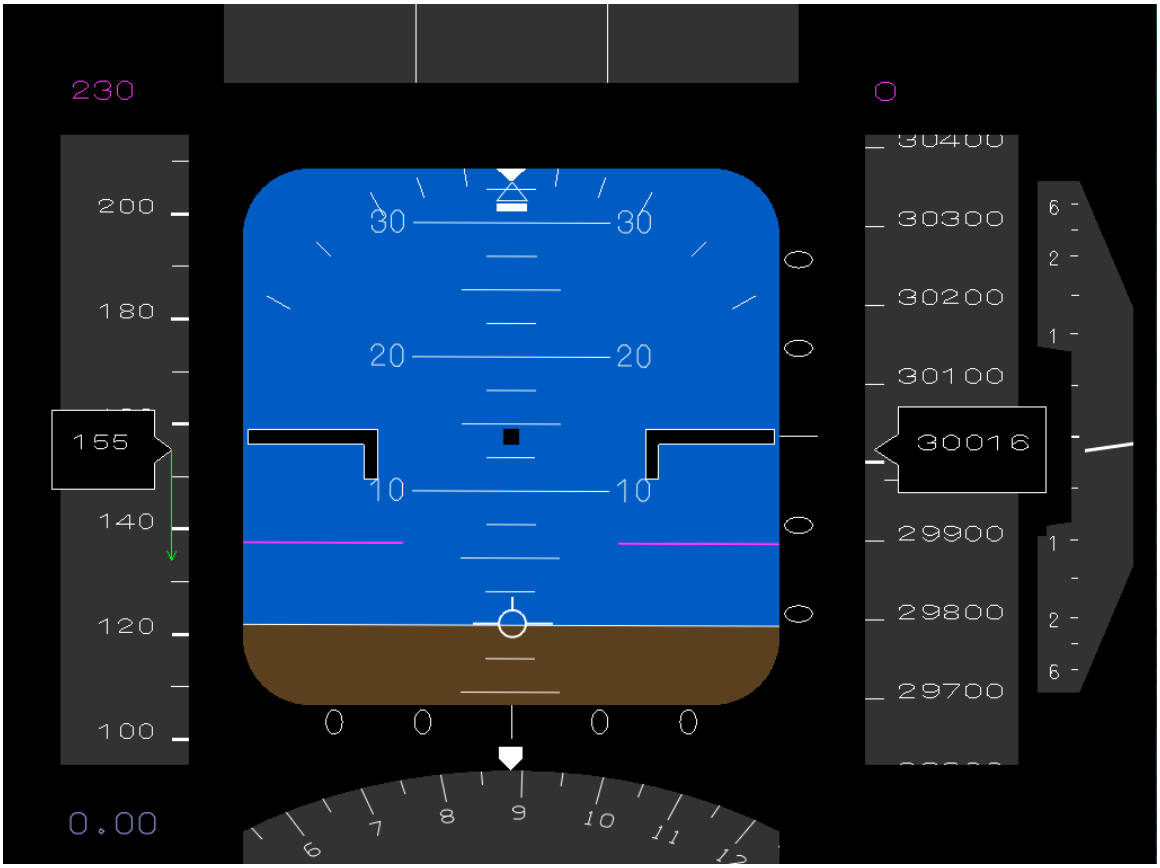

Fig. 7 PFD with the pitch angle guidance signal (magenta line) in approach to stall condition.

$q_{com}(t)$ computed according to (33).

- Generate the comparison signal $w_u(t)$.
- If $q_{com}(t_u) \geq w_u(t_u) + f(x, \alpha_{guid})$, run the reference model (38) with $\alpha_{ref}(t_u) = \alpha_{guid}(t_u)$, and set $q_{com}(t) = -k_\alpha[\alpha_{ref}(t) - \alpha_t] + f(x, \alpha_{guid})$.
- Generate $\theta_{guid}(t)$ according to (40) and display on the PFD.
- Generate the comparison signal $w_l(t)$.
- If $q_{com}(t_l) \leq w_l(t_l) + f(x, \alpha_{guid})$, reset $q_{com}(t)$ to (33) and the guidance model initial condition to $\alpha_{guid}(t_l) = \alpha(t_l)$.
- Remove $\theta_{guid}(t)$ from the PFD.

V. Simulation Results

We evaluate the stall recovery guidance algorithms using the Transport Class Model (TCM) as defined in [16] and the pilot-in-the-loop FLTz simulation environment available in the Advanced Control Technologies (ACT) lab at NASA Ames Research Center. For this simulations, we assume that the TCM is in a steady level flight at the altitude of 30000 ft with the calibrated airspeed of $230kt$ when an engine control malfunction results in the minimal throttle settings, but the autopilot still works in the altitude hold mode. This is similar to Air Algerie Flight 5017 (MD-83) crash in Mali, near Gossi, on 24 July 2014, caused by the engine pressure sensors icing, which resulted in the autothrottle disengagement.

Since the aircraft gradually slows down, the autopilot increases the pitch angle in order to maintain the altitude, which eventually results in stall. In these simulation experiments the aircraft flies without the autopilot, but the pilot is tasked to maintain the level flight, thus mimicking the autopilot in the altitude hold mode. When the aircraft gets into the stall, the pilot's task is to recover from the stall by following the displayed guidance signal and then maintain level flight afterworlds. In all simulations, for the guidance algorithms the maximum angle of attack is set to 14 deg, which is close to the aircraft stall angle.

Analysis of the available data indicates that the crew likely did not activate the system during climb and cruise.

As a result of the icing of the pressure sensors, the erroneous information transmitted to the autothrottle meant that the latter limited the thrust delivered by the engines. EPR fluctuations on both engines started, followed by two variations of greater amplitude. The autothrottle disengaged during these two variations in EPR and the aeroplane started to descend.

In the first simulation experiment the pilot was tasked to follow the flight path angle guidance (FPAG) signal to recover from the stall. Figure 2 displays the PFD at the initial conditions. The FPAG signal is represented by a magenta circle inside the flight path symbol (white circle with the wings), which implies that $\gamma_{guid}(t)$ and $\gamma(t)$ are identical for the initial value of the angle of attack. As the aircraft approaches to stall the magenta circle separates from the flight path symbol and moves downward as it can be seen from Figure 3, indicating that a safe maneuver would be

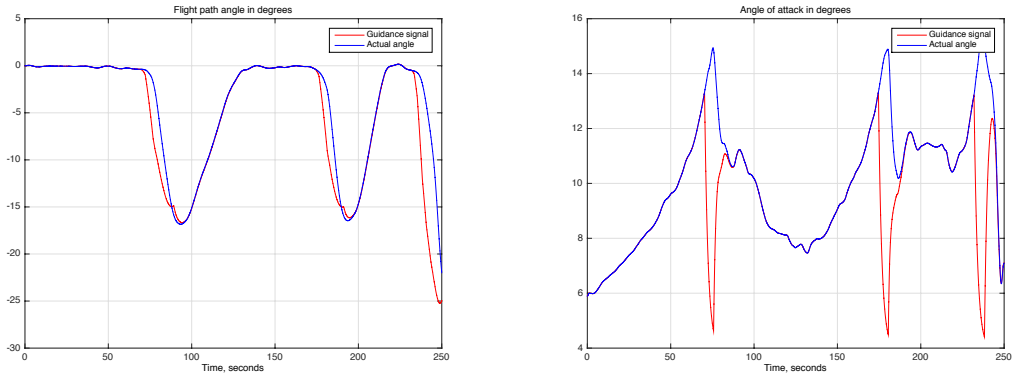

(a) FPAG and actual flight path angle time histories (b) Computed from the SL algorithm and actual angles of attack time histories

Fig. 8 Displayed guidance signal and the angle of attack when the pilot follows FPAG

generating a negative flight path angle.

The pilot pitches down and follows the magenta circle to recover the aircraft. Figure 8(a) displays the flight path angle time history. It can be observed that stall happens at about $t = 70$ *sec*, and the pilot starts to follow the guidance signal in 3 *sec*. The aircraft gets out of stall very fast, but the pilot starts gradually recovering the aircraft at $t = 96$ *sec*. The second stall happens at about 175 *sec*, and the pilot follows the guidance signal and quickly recovers the aircraft second time as it can be observed from Figure 8(b), which displays the actual angle of attack (blue line) and $\alpha_{guid}(t)$ signal computed by the state limiting guidance (SLG) algorithm. The corresponding $\theta_{guid}(t)$ signal along with the actual pitch angle response are presented in Figure 9(a). Although $\theta_{guid}(t)$ was not displayed on PFD for this experiment, it can be observed that pitch angle guidance (PAG) signal leads the FPAG signal for about a second. This can be explained by the anticipatory nature of the state limiting approach, since the derivative of the desired angle of attack is regulated. The altitude guidance (AG) signal was also computed in the background. It is displayed in Figure 9(b). It can be noticed that the AG is lagging behind the FPAG for about a second, which is attributed to higher order dynamics for generation of the AG signal.

In the second experiment only the AG signal was displayed to the pilot performing the same task from the same initial conditions as in the first case. Figures 10(a) and 10(b) display the altitude and the corresponding angle of attack time histories. It can be seen that the pilot was able to

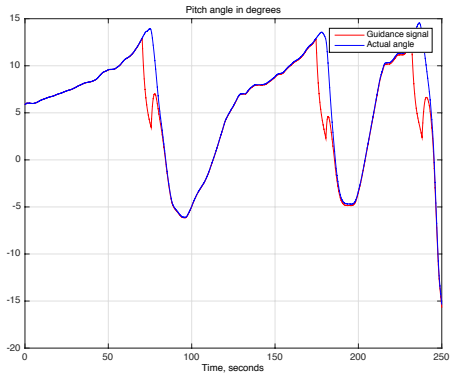

(a) PAG and actual pitch angle time histories

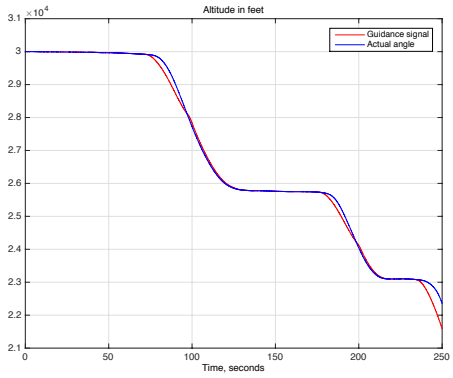

(b) AG and actual altitude time histories

Fig. 9 Computed but not displayed signals when the pilot follows FPAG

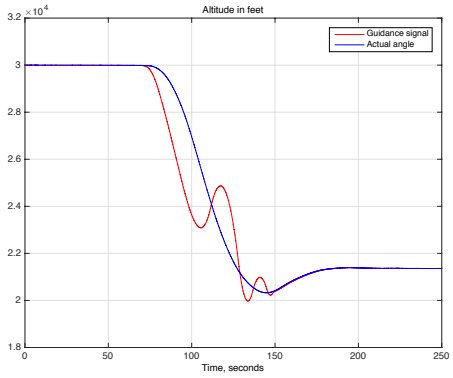

(a) AG and actual altitude time histories

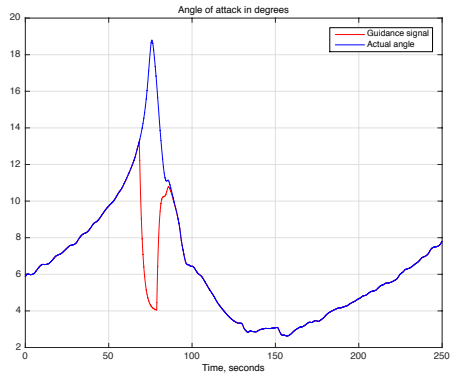

(b) Computed from the SL algorithm and actual angles of attack time histories

Fig. 10 Displayed guidance signal and the angle of attack when the pilot follows AG

recover from the stall following the AG signal, although it gives the recovery cue slower than the other two algorithms as it can be learn from Figures 11(a) and 11(b). Namely, the stall is predicted by AG algorithm at $t = 72$ second, while FPAG detects it at $t = 70$ seconds, and AG detects it at $t = 69$ seconds. Additionally, it can be observed from Figure 11(a) that FPAG algorithm is more conservative and suggests a dipper dive for the recovery.

In the third experiment the pilot performs the same task following the PAG signal from the same initial conditions as in the previous cases. Figures 12(a) and 12(b) display the pitch angle and the corresponding angle of attack time histories. It can be observed that the PAG algorithm generate non-smooth pitch angle guidance (red line in Figure 12(a)) and desired angle of attack (red

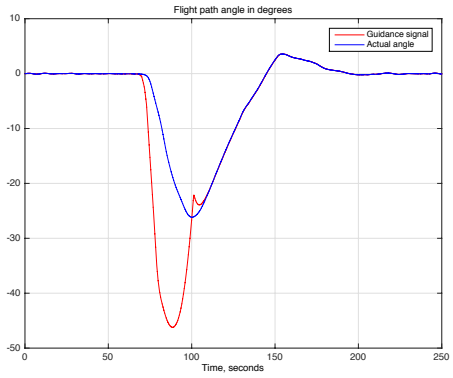

(a) FPAG and actual flight path angle time histories

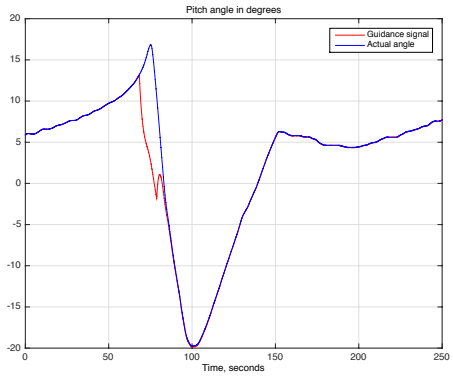

(b) PAG and actual pitch angle time histories

Fig. 11 Computed but not displayed signals when the pilot follows AG

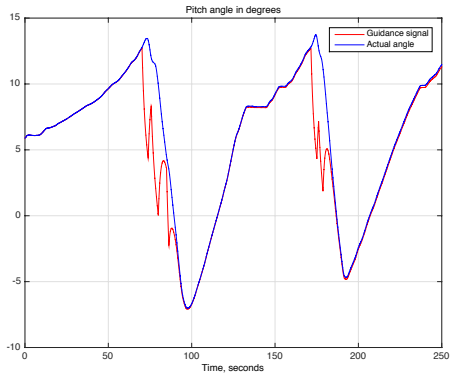

(a) PAG and actual pitch angle time histories

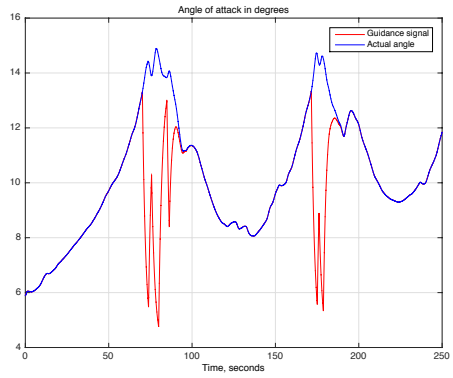

(b) Computed from the SL algorithm and actual angles of attack time histories

Fig. 12 Displayed guidance signal and the angle of attack when the pilot follows PAG

line in Figure 12(b)) signals due to switches in the desired angle of attack dynamics. However, the PAG signal gives the recovery cue to the pilot earlier that the guidance signals generated by the FPAG and AG algorithms as it is evident from Figures 13(a) and 13(b) respectively. Also, it can be learned from these figures that FPAG and AG algorithms suggest a dipper dive in order to recover from the stall.

These simulation experiments show that the PAG algorithm gives more lead time to the pilot than the other two algorithms, but generate non-smooth guidance signal. The FPAG algorithm generates smoother but conservative signal requiring a dipper dive. The AG algorithm is slower than other two algorithms and results in most altitude loss during the recovery maneuvers. However,

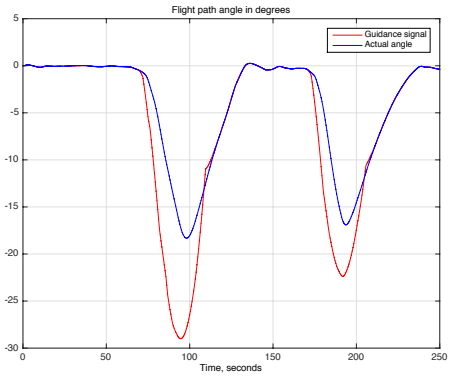

(a) FPAG and actual flight path angle time histories

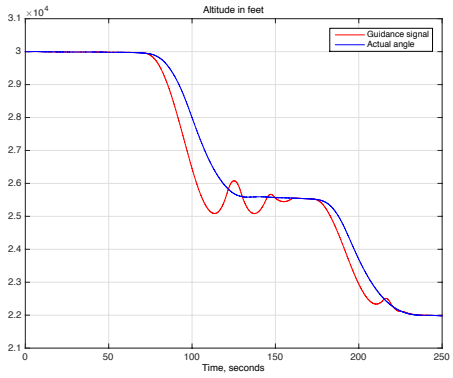

(b) AG and actual altitude time histories

Fig. 13 Computed but not displayed signals when the pilot follows PAG

these are only preliminary results, and more research and analysis are needed in order to improve the algorithms from the perspective of the pilots perception and aircraft performance criteria such as minimum altitude loss or time to recover, before the algorithms can be evaluated in piloted simulations in the NASA Ames Research Center Vertical Motion-based Simulation facility.

VI. Conclusion

We have presented several aircraft stall recovery guidance algorithms based on the input and state constraint control approaches. These algorithms are implemented as plug-and-play technology, which do not interfere with the flight control system and do not modify the pilot's actions. The outputs of the algorithms are provided to the pilot in the form of visual signals on the Primary Flight Display when the aircraft is in stall or approach to stall. The pilot has the ultimate power to follow the guidance signals. The algorithms are validated in the pilot-in-the loop high fidelity simulation experiment.

References

[1] D. R. Gingras abd J. N. Ralston, R. Oltman, C. Wilkening, R. Watts, and P. Derochers. Flight Simulator Augmentation for Stall and Upset Training (AIAA 2014-1003). *In Proceedings of the AIAA Modeling and Simulation Technologies Conference*, 2014.

[2] Federal Aviation Administration. Stall and Stick Pusher Training. *Advisory Circular, Washington DC*, (120-109), August 2012.

[3] Federal Aviation Administration. Qualification, Service, and Use of Crewmembers and Aircraft Dispatchers; Final Rule, 14 CFR Part 121. *Federal Register, http://www.gpo.gov/fdsys/pkg/FR-2013-11-12/pdf/2013-26845.pdf*, 78(218), Novenber 12 2013.

[4] J. S. Barlow, V. Stepanyan, and K. Krishnakumar. Estimating Loss-of-Control: a Data-Based Predictive Control Approach. *In Proceedings of the AIAA Guidance, Navigation, and Control Conference, Portland, OR*, August 2011.

[5] C. M. Belcastro. Loss of Control Prevention and Recovery: Onboard Guidance, Control, and Systems Technologies. *In Proceedings of the AIAA Guidance, Navigation, and Control Conference, Minneapolis, MN*, August 2012.

[6] M.T. Bement and S. Jayasuriya. Construction of a Set of Nonovershooting Tracking Controllers. *Journal of Dynamic Systems, Measurement and Control*, 126(3):558–567, 2004.

[7] J. Chongvisal, N. Tekles, E. Xargay, D. A. Talleur, A. Kirlikk, and N. Hovakimyan. Loss-of-Control Prediction and Prevention for NASA's Transport Class Model. *In Proceedings of the AIAA Guidance, Navigation and Control Conference, National Harbor, MD*, January 2014.

[8] D. Crider. Accident Lessons for Stall Upset Recovery Training. *In Proceedings of the AIAA Guidance, Navigation, and Control Conference*, 2010.

[9] S. Darbha and S. P. Bhattacharyya. On the Synthesis of Controllers for a Nonovershooting Step Response. *IEEE Transactions on Automatic Control*, 48(5):797–799, May 2003.

[10] R. L. M. El-Khoury and O.D. Crisalle. Influence of Zero Locations on the Number of Step-response Extrema. *Automatica*, 29:1571–1574, 1993.

[11] J. A. A. Engelbrecht, S. J. Pauck, and Iain K. Peddle. A Multi-Mode Upset Recovery Flight Control System for Large Transport Aircraft. *In Proceedings of the AIAA Guidance, Navigation, and Control Conference, Boston, MA*, August 2013.

[12] R. Gadient, E. Lavretsky, and D. Hyde. State Limiter for Model Following Control Systems, AIAA 2011-6483. *In Proceedings of the AIAA Guidance, Navigation, and Control Conference, Portland, OR*, August 2011.

[13] S. J. Gill, M. H. Lowenberg, S. A. Neild, B. Krauskopf, G. Puyou, and E. Coetzee. Upset Dynamics of an Airliner Model: A Nonlinear Bifurcation Analysis. *Journal Of Aircraft*, 50(6), 2013.

[14] N. Govindarajan, C. C. de Visser, E. van Kampen, K. Krishnakumar, J. Barlow, and V. Stepanyan. Framework for Estimating Autopilot Safety Margins. *Journal Of Guidance, Control, And Dynamics*, 37(4), 2014.

[15] J. Guo, Y. Liu, and G. Tao. A Multivariable MRAC Design Using State Feedback for Linearized

Aircraft Models with Damage. *In Proceedings of the American Control Conference, Baltimore, MD*, 2010.

[16] R. M. Hueschen. Development of the Transport Class Model (TCM) Aircraft Simulation From a Sub-Scale Generic Transport Model (GTM) Simulation. *NASA/TM 2011-217169*, August 2011.

[17] E. N. Johnson. *Limited Authority Adaptive Flight Control, Ph.D. thesis*. Georgia Institute of Technology, 2000.

[18] A. Khelassi, D. Theilliol, P. Weber, and J.-C. Ponsart. Fault-tolerant control design with respect to actuator health degradation: An LMI approach. *In Proceedings of the IEEE Multi-Conference on Systems and Control, Denver, CO*, 2011.

[19] D. K. Kufoalor and T. A. Johansen. Reconfigurable Fault Tolerant Flight Control based on Nonlinear Model Predictive Control. *In Proceedings of the American Control Conference, Washington, DC*, 2013.

[20] H. G. Kwatny, J.-E. T. Dongmo, B.-C. Chang, G. Bajpai, M. Yasar, and C. Belcastro. Nonlinear Analysis of Aircraft Loss of Control. *Journal Of Guidance, Control, And Dynamics*, 36(1), 2013.

[21] T. Lombaerts, G. Looye, P. Chu, and J. A. Mulder. Pseudo Control Hedging and its Application for Safe Flight Envelope Protection. *AIAA paper AIAA-2010-8280*, 2010.

[22] T. J. J. Lombaerts, S. R. Schuet, K. R. Wheeler, D. M. Acosta, and J. T. Kaneshige. Safe Maneuvering Envelope Estimation Based on a Physical Approach. *In Proceedings of the AIAA Guidance, Navigation and Control Conference, Boston, MA*, August 2013.

[23] W. MacKunis, P. M. Patre, M. K. Kaiser, and W. E. Dixon. Asymptotic Tracking for Aircraft via Robust and Adaptive Dynamic Inversion Methods. *IEEE Transactions on Control Systems Technology*, 18, 2010.

[24] K. McDonough, I. Kolmanovsky, and E. Atkins. Recoverable Sets of Initial Conditions and Their Use for Aircraft Flight Planning After a Loss of Control Event. *In Proceedings of the AIAA Guidance, Navigation and Control Conference, National Harbor, MD*, January 2014.

[25] P K. Menon, P. Sengupta, S. Vaddi, B.-J. Yang, and J. Kwan. Impaired Aircraft Performance Envelope Estimation. *Journal of Aircraft*, 50:410–424, 2013.

[26] E. A. Morelli, K. Cunningham, and M. A. Hill. Global Aerodynamic Modeling for Stall/Upset Recovery Training Using Efficient Piloted Flight Test Techniques (AIAA 2013-4976). *In Proceedings of the AIAA Modeling and Simulation Technologies (MST) Conference*, 2013.

[27] The Bureau of d'Enquetes et d'Analyses (BEA) pour la securite de l'avation civile. Final Report: On the accident on 1 June 2009 to the Airbus A330-203 registered F-GZCP operated by Air France flight 447 Rio de Janeiro-Paris. July 2012.

[28] R. C. Paul, J. Murua, and A. Gopalarathnam. Unsteady and Post-Stall Aerodynamic Modeling for Flight Dynamics Simulation (AIAA 2014-0729). *In Proceedings of the AIAA Atmospheric Flight Mechanics Conference*, 2014.

[29] T. Peni, B. Vanek, Z. Szabo, P. Gaspr, and J. Bokor. Supervisory Fault Tolerant Control of the GTM UAV Using LPV Methods. *In Proceedings of the Conference on Control and Fault-Tolerant Systems, Nice, France*, 2013.

[30] National Transportation Safety Board Accident Report. Loss of Control on Approach Colgan Air, Inc. Operating as Continental Connection Flight 3407 Bombardier DHC-8-400. *Report Number NTSB/AAR-10/01, PB2010-910401, N200WQ Clarence Center, NY*, February 2009.

[31] R. Schmid and L. Ntogramatzidis. On the Design of Non-overshooting Linear Tracking Controllers for Right-invertible Systems. *In Proceedings of the IEEE Conference on Decision and Control, Shanghai, China*, 2009.

[32] J. Schroeder. An Evaluation of Several Stall Models for Commercial Transport Training, AIAA 2014-1002. *In Proceedings of the AIAA Modeling and Simulation Technologies Conference, National Harbor, MD*, January 2014.

[33] P. Shankar. Characterization of Aircraft Trim Points Using Continuation Methods and Bifurcation Analysis. *In Proceedings of the AIAA Guidance, Navigation and Control Conference, Boston, MA*, August 2013.

[34] V. Stepanyan, K. Krishnakumar, J. Barlow, and H. Bijl. Adaptive Estimation Based Loss of Control Detection and Mitigation. *In Proceedings of the AIAA Guidance, Navigation and Control Conference, Portland, OR, AIAA 2011-6609*, August 2011.

[35] Y. Tang and R. J. Patton. Reconfigurable Fault Tolerant Control for Nonlinear Aircraft based on Concurrent SMC-NN Adaptor. *In Proceedings of the American Control Conference, Portland, OR*, 2014.

[36] Commercial Aviation Safety Team. Safety Enhancement SE 207, Attitude and Energy State Awareness Technologies. *http://www.skybrary.aero/bookshelf/books/2538.pdf*, December 2013.

[37] N. Tekles. *Flight Envelope Protection and Loss-of-Control Prevention for NASA's Transport Class Model.* Technical University Munich, 2014.

[38] N. Tekles, E. Xargay, R. Choe, N. Hovakimyan, I. M. Gregory, and F. Holzapfel. Flight Envelope Protection for NASA's Transport Class Model. *In Proceedings of the AIAA Guidance, Navigation and Control Conference, National Harbor, MD*, January 2014.

[39] H. Wu and F. Mora-Camino. Glide Control for Engine-Out Aircraft. *In Proceedings of the AIAA*

Guidance, Navigation, and Control Conference, Minneapolis, MN, August 2012.

[40] W. Yao, Y. Lingyu, Z. Jing, and Shen Gongzhang. An Observer Based Multivariable Adaptive Reconfigurable Control Method for the Wing Damaged Aircraft. *In Proceedings of the IEEE International Conference on Control and Automation, Taichung, Taiwan*, 2014.

[41] S. Schuet znd T. Lombaerts, D. Acosta, K. Wheeler, and J. Kaneshige. An Adaptive Nonlinear Aircraft Maneuvering Envelope Estimation Approach for Online Applications. *In Proceedings of the AIAA Guidance, Navigation and Control Conference, National Harbor, MD*, January 2014.